Drop impact onto a solid sphere: the case of hydrophobic and superhydrophobic surfaces and low Weber numbers.

Danial Khojasteh[1], Reza Kamali[2], Marco Marengo[3]
[1]Water Research Laboratory, School of Civil and Environmental Engineering, UNSW Sydney, NSW, Australia - danial.khojasteh@unsw.edu.au
[2]School of Mechanical Engineering, Shiraz University, Shiraz 71936-16548, Iran - rkamali@shirazu.ac.ir
[3]School of Computing, Engineering and Mathematics, University of Brighton, Brighton BN2 4GJ, UK
*Corresponding author: m.marengo@brighton.ac.uk

Abstract
Encapsulation of solid particles and liquid agents in a liquid shell is of exceptional interest in biotechnological, chemical and pharmaceutical fields such as personalized medicine, fluidized catalytic cracking, wire fabrication, catalytic reactions. Looking at the interaction between liquid drop and solid particles, we can study the special, ideal case of spherical drops impacting solid spheres, in order to understand the basic phenomena and the effect of the physical variables on the spreading behavior. Considering the importance of dynamics of drop-particle collision, which directly affects the quality of film deposition during encapsulation, various aspects of drop impact on dry solid spherical surfaces are still lacking in the existing literature. The cases are studied with a 3D level-set method implemented in a standard finite-element-based solver platform. The impact Weber number, the size ratio (ratio of spherical particle diameter to droplet diameter), and the surface contact angle (CA) are varied throughout the numerical simulations within a suitable range. After providing a strong validation with experimental data, it is found that impact on spherical surfaces generally presents a higher area of liquid to be in contact with the substrate with respect to the case of flat surfaces, when all other impact conditions are the same. The maximum spreading diameter increases with the impact velocity, with an increase of the sphere diameter, for a lower surface wettability and a lower surface tension. Typical outcomes of the impact include 1) complete rebound, 2) splash, and 3) final deposition stage after a series of spreading and recoiling phases. The roles of the centrifugal and the gravitational forces are considered and quantified. Finally, a model is proposed, which can reasonably predict the maximum deformation of low Reynolds number impact of droplets onto hydrophobic (H) or superhydrophobic (SH) spherical solid surfaces.

Keywords
Encapsulation, wettability, multiphase flows, level-set method.

Introduction

While a vast number of numerical, analytical and experimental investigations are dedicated to droplet dynamics after hitting a planar surface [1,2], the current literature is limited in understanding this impact on non-planar surfaces (i.e., spherical surfaces) despite the high number of applications of this process in industrial, biotechnological, chemical and pharmaceutical fields [3,4]. To illustrate, droplet-particle collision is significant in process industries during heterogeneous catalytic reactions and wetting of catalyst particles [5]. Brackish water from seas are sprayed on arrays of tubes (carrying hot water) in multi-effect desalination evaporators to produce distilled water. This phenomenon has also attracted a great deal of attention in droplet-based microfluidics, where numerous techniques are being developed to manipulate and functionalise droplet impingement [6]. The encapsulation process provides a powerful tool for various industrial applications including in biotechnological, chemical and pharmaceutical fields. For example, droplets which are encapsulated with H particles are extensively used in microreactors, gas sensing, and water pollution discovery [7]. The so-called spray drying is widely applied to achieve encapsulation because it provides good flexibility and a continuous operation [8]. This procedure is a conventional method of converting feedstock from a fluid state to dried particles through spraying the coating agent on the particles in which the sprayed droplets spread on the surface of the particles [8]. Then, the particles are heated by a flow of hot air to attain a swift liquid evaporation. In ideal case, the target particles need to be dense, and have spherical shape as well as high wettability to keep the momentum exchange of droplet particle and coating material to a minimum. For an effective encapsulation operation, the spreading of encapsulating material should be controlled, and a successful droplet landing should be gained to avoid splashing or bouncing of the droplets [9].

Based on our exhaustive literature review and previous papers in this field [5,6,8], it is found that the majority of research about droplets undergoing collision with particles are carried out for 2D non-bouncing cases and 3D modelling of bouncing cases requires careful attention. Further, a gap exists among the pre-established relations for predicting the maximum spreading diameter of droplet after impacting spherical surfaces. While the dynamics of droplet-particle impact significantly influences the quality of film deposition during encapsulation process, various aspects of drop impact onto dry solid spherical surfaces are still missing in the existing literature. To bridge these gaps, a series of 3D simulations are performed to model droplet impact onto H and SH spherical surfaces by taking level set method to examine the effects of impacting Weber (*We*) number (through changing impact velocity and surface tension), surface wettability in terms of contact angle (CA), and the size ratio of the solid surface to the droplet diameter ($D^* = d_{sphere}/d_{drop}$).

Mathematical modelling

The continuity and the momentum equations are solved to obtain the flow field as below [10]:

$$\nabla.\vec{u} = 0 \tag{1}$$

$$\rho\left(\frac{\partial\vec{u}}{\partial t} + \vec{u}\cdot\nabla\vec{u}\right) = -\nabla p + \nabla\left(\mu(\nabla\vec{u} + (\nabla\vec{u})^T)\right) + \rho\vec{g} + \sigma\kappa\delta\vec{n} + \vec{F} \tag{2}$$

The above equations are coupled with level set equation to track the changes in fluid interface. This equation is defined as [11]:

$$\frac{\partial\Phi}{\partial t} + \vec{u}\cdot\nabla\Phi = \gamma[\nabla\cdot(\varepsilon\nabla\Phi - \Phi(1-\Phi)\frac{\nabla\Phi}{|\nabla\Phi|})] \tag{3}$$

These equations are solved together using a numerical finite-element-based solver platform.

Model validation and definition

To validate the accuracy of numerical simulations, several cases with available experimental data are compared to the obtained results from our numerical platform and the results independency from mesh and grid generations are checked in our previous papers [5,6]. As an example, a plot of the normalized diameter (ratio of drop diameter at any instant to its initial diameter) of the drop versus time is depicted in Figure 1, in which the numerical simulations are compared against experimental data presented by Wang et al. [12] for a water droplet impacting a SH surface with equilibrium CA of 163°, and the impact velocity of 0.56 m/s. As is clear from the figure, acceptable accuracy exists in predicting the spreading diameter of droplet hitting an SH surface.

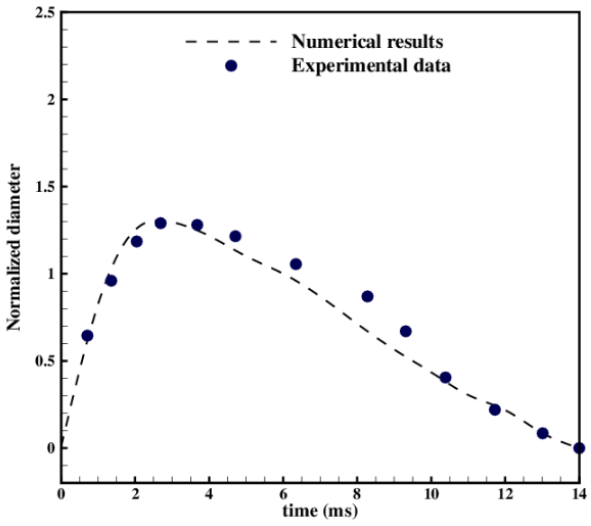

Figure 1. A comparison of normalized diameter versus time between obtained results from current numerical study and experimental data reported by Wang et al. [12].

For all simulated cases in this study, a perfectly circular water droplet is assumed right at the top of the spherical particle, having a downward velocity. The initial diameter of droplet is 2.3 mm, impacting onto H and SH surfaces with CAs of 125° and 163°, respectively. The ratio of the solid sphere diameter to the droplet diameter D* ranges from 1 to 8, and the impact *We* number is varied from 5 to 30. The physical properties of water droplet and surrounding air are as follows; water dynamic viscosity is 0.001 Pa.s, water density is 998 kg/m^3, air dynamic

viscosity is $1.81*10^{-5}$, air density is 1.2 kg/m^3, and surface tension between water and air phases is 0.072 N/m. The use of the constant equilibrium contact angle, instead of a more complete model which may consider the advancing and receding contact angle, for example using the Kistler equation, is allowable by the fact that in practical case such surfaces have a low contact angle hysteresis, and the focus of our work on the spreading up to its maximum extension.

Results and discussion

In order to show the effects of surface wettability (in terms of CA) and *We* number by varying impact velocity, Figure 2 indicates the normalized spreading diameter ($d_{lamella}/d_{drop}$) for water droplet hitting H and SH spherical particles when D*=6. According to this figure, a lower CA presents a greater normalized diameter, and hence, a higher spreading diameter (longer duration for the spreading phase). This finding agrees with the experimental data on drop impact on flat surfaces such as those reported by [13]. This figure also illustrates the influence of impact velocity by increasing *We* number from 5 to 30. As expected, there is a significant increase in the maximum spreading diameter with rising *We* numbers for both CA values, which is due to the higher kinetic energy of the impacting droplet. Further, the recoiling stage is generally shorter with increasing impact velocity as this higher velocity leads to a higher velocity of receding as reported by [14]. This, in turn, causes the droplet to reach the maximum spreading in a shorter period for higher *We* numbers.

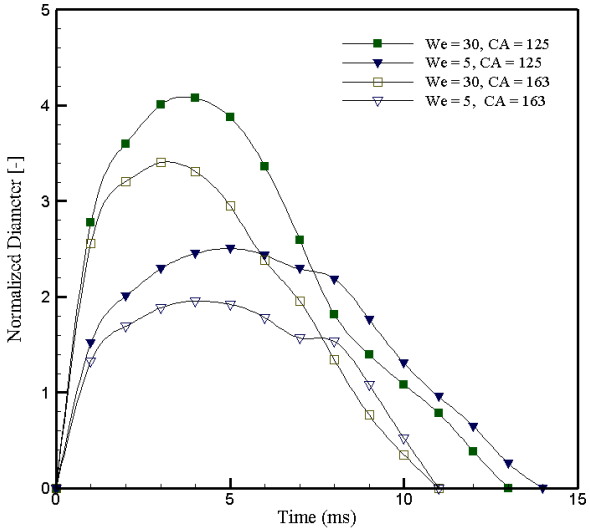

Figure 2. Normalized diameter with respect to time at different CAs and *We* numbers for D*=6.

Figure 3 shows the normalized diameter for a water droplet collides with H and SH particles for *We*=15 and D* varies from 2 to 6. As observable, there is an increase in the spreading stage, and hence a relatively larger proportion of the solid particle is wetted by the droplet for lower values of D*. Moreover, bigger spherical particles are associated with a shorter contact time with droplet. For impact on SH particles, the impact time increases by 1 ms as D* shifts from 6 to 2.

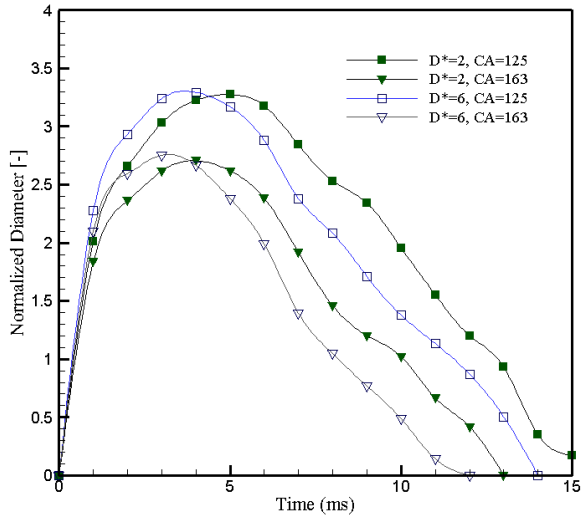

Figure 3. Normalized diameter with respect to time for drop impact onto H and SH particles with different surface-to-droplet size ratios when *We*=15.

To better understand the effect of size ratio, Figure 4 presents the time-lapsed images of droplet impacting SH particles when *We*=15. It is apparent that droplet breaking down or splashing are not occurring in these cases, and the drop first turns into a pancake shape follows by a retraction and bouncing off the surface.

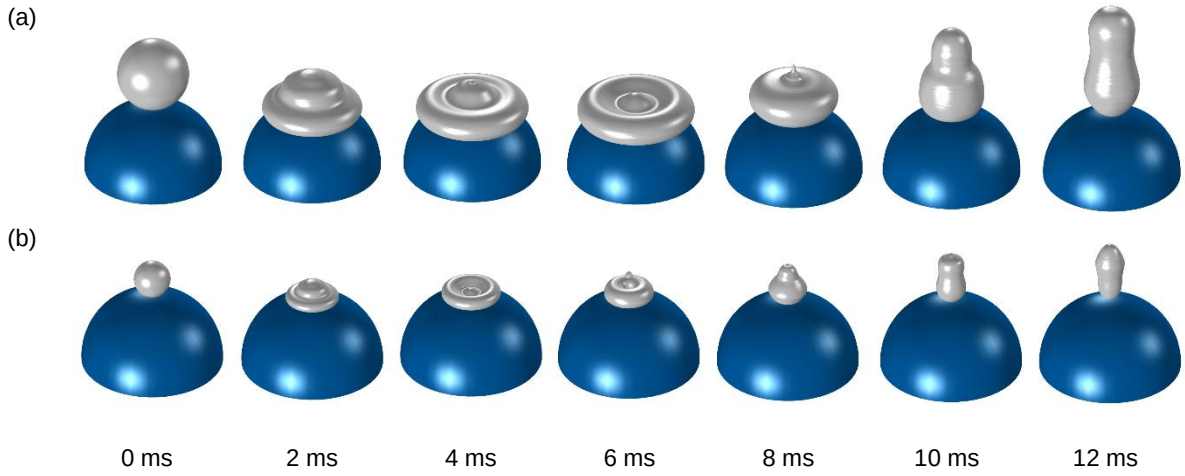

Figure 4. Time-lapsed evolution of droplet impacting SH particles when *We*=15 for: (a) D*=2, and (b) D*=4.

Figure 5 demonstrates the effect of *We* number by changing surface tension (γ), which is a key factor in determining whether a droplet bounces off the surface after impact or not, for *We*=5 and CA=125°. Recognising that such CAs are very difficult to achieve for a low surface tension fluid, here a synthetic fluid is introduced which has a surface tension of 0.018 N/m, while its other properties are like those of water in previous cases. A considerable change in droplet shape deformation is observable by decreasing surface tension, following with higher values of maximum spreading. Additionally, an interesting phenomenon occurs when applying lower values of surface tension in which the normalized diameter achieves a minimum value, but the droplet starts spreading again afterwards. The reason behind is that fewer energy is stored as surface energy and then is converted to kinetic energy during the receding phase when using a smaller surface tension and hence, the released surface energy is not enough to assist in rebound stage [6,14].

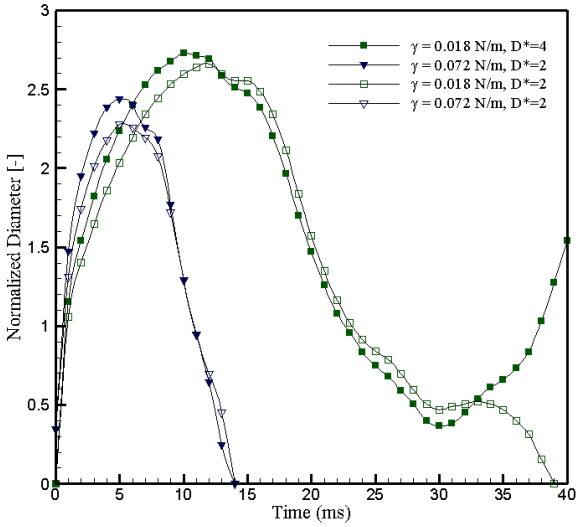

Figure 5. Normalized diameter with respect to time for impacts onto H particles with different surface-to-droplet size ratios and surface tensions when *We*=5.

The maximum spreading diameter is a prominent factor in numerous industrial applications (e.g., inkjet printing). Several researchers tried to provide correlations to predict this parameter by using dimensionless numbers such as *We* and Reynolds (*Re*) numbers among which are [15-18]. All these correlations are developed based on drop impacting onto planar surfaces. However, based on our numerical simulations, impact on spherical particles experiences a higher area of liquid to be in contact with the surface with respect to the case of flat surface, which is due to additional forces exert on droplet including gravity and centrifugal forces [5]. In order to quantify the roles of gravitational and centrifugal forces, a parameter named α is introduced as the ratio of centrifugal force to

gravitational one. The definition is presented based on the forces acting on a generic volume of liquid at the rim and is defined as [5]:

$$\alpha = \frac{F_{centrifugal}}{F_{gravity}} = \frac{V_{sp}^2}{gR \cdot tan\,(\frac{l}{R})} \quad (4)$$

The plot of this ratio is depicted in Figure 6, indicating that the role of centrifugal force is certainly of a higher level of influence than gravity one, and is the main factor that droplet spreading on spherical surfaces is greater than that of flat ones.

As mentioned above, the available correlations in the literature are incapable of predicting the maximum spreading diameter for impacts onto spherical objects. In this study, a spreading factor (β) is introduced as the ratio of the maximum spreading diameter (D_{max}) of the droplet by its initial diameter (D_0). The results of the comparison of spreading factor for the flat and the spherical H and SH surfaces are indicated in Figure 7. It is clear that the spreading factor is higher for impact on spherical particles and available correlations cannot predict this factor for impact on non-planar surfaces especially for H spherical surfaces. Furthermore, through simulating several cases and doing a comprehensive analysis for impacts of water droplets on spherical H and SH surfaces with D* varies from 1 to 8 and *We* number changes from 5 to 30, a novel correlation is proposed to predict the maximum spreading factor (β_{max}) for impact of low viscosity fluids onto spherical particles and for *We* numbers up to 30 as below [6]:

$$\beta_{max} = 1.54We^{0.3}(3.52 - \theta)^{0.25} \quad (5)$$

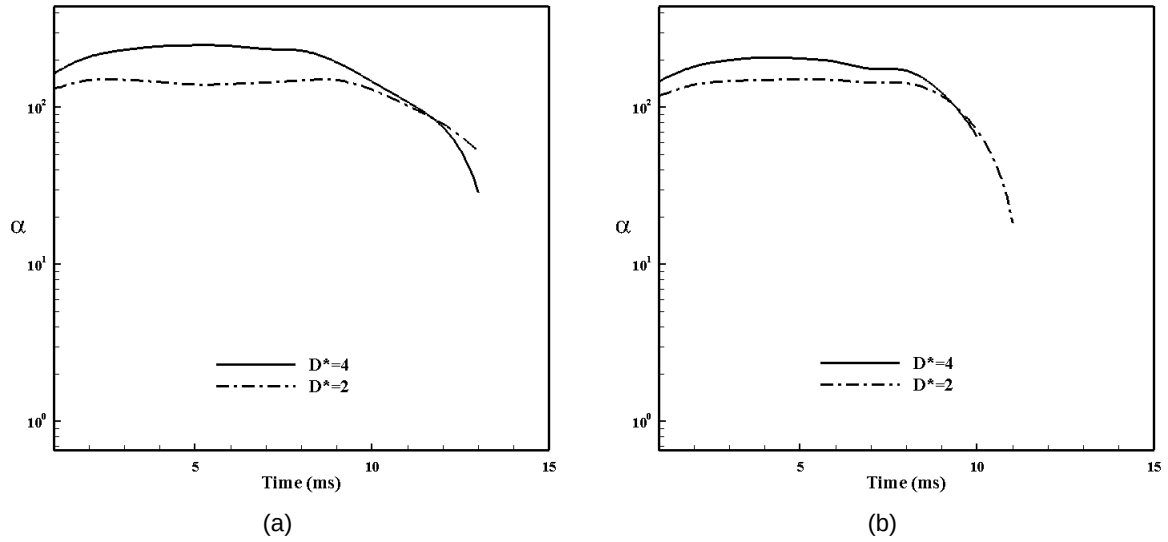

Figure 6. The ratio of centrifugal force to gravitational one with respect to time for: (a) H, and (b) SH surfaces.

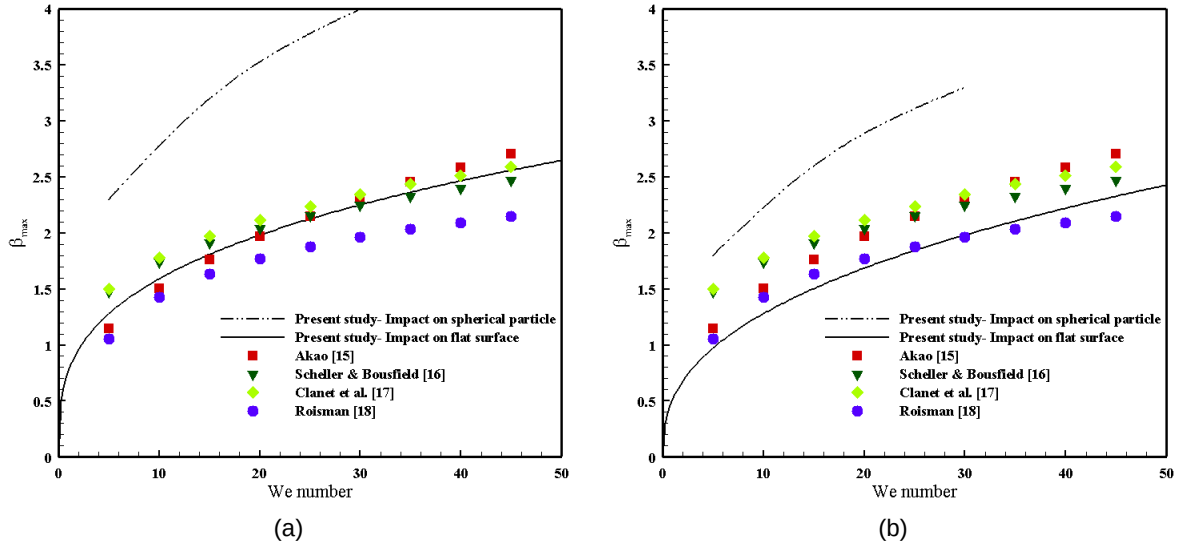

Figure 7. Comparison of obtained maximum spreading factor to available correlations for: (a) H, and (b) SH surfaces.

Conclusions

This paper presents 3D level-set simulations of drop impacts onto spherical particles, in order to understand the physical behaviour of the basic mechanisms of particle encapsulation. Impact outcomes include complete rebound, splash, and deposition. For a given impact condition, impacts on spherical solid particles present a larger area of liquid in contact with the substrate. As expected, the maximum spreading diameter increases with the impact velocity, with an increase of the contact angle and a lower surface tension, but also with an increase of the sphere diameter. The roles of the centrifugal and the gravitational forces are considered and quantified to explain such variations. A model is proposed, which predicts the maximum deformation of low Reynolds number impact of droplets onto hydrophobic (H) or superhydrophobic (SH) spherical solid surfaces. The model may find a technical relevance in the field of particle coating and production of marble drops, limited to the cases when the variation of the particle momentum is not important and the motion of both the particles and the drops is not strongly influenced by the flow around.

Acknowledgements

The authors would like to thank Alireza Bordbar from Shiraz University for his contribution in preparing the simulation cases for this study.

Nomenclature

CA	Contact angle
D_0	Droplet initial diameter
D_{max}	Droplet maximum spreading diameter
D*	Ratio of particle's diameter to drop's diameter
F	External forces
g	Gravitational acceleration
H	Hydrophobic
k	Local curvature of the fluid-fluid interface
l	Semi-length of the spreading
n	Unit normal vector to the interface
R	Particle radius
Re	Reynolds number
SH	Superhydrophobic
u	Velocity vector
Vsp	Spreading velocity
We	Weber number
α	Ratio of centrifugal force to gravitational force
β	Ratio of D_{max} to D_0
ρ	Density
γ	Surface tension
θ	Equilibrium contact angle in radians
Φ	Level set function
μ	Dynamic viscosity

References

[1] Khojasteh, D., Mousavi, S.M., Kamali, R., 2017, Indian Journal of Physics, 91 (5), pp.513-520.
[2] Kamali, R., Khojasteh, and D., Mousavi, S.M., April 26-28. 2016, Newtonian and Non-Newtonian Droplet Impact onto a Heated Hydrophobic Solid Surface. 24th Annual International Conference on Mechanical Engineering-ISME, Yazd, Iran.
[3] Bordbar, A., Taassob, A., Zarnaghsh, A., Kamali, R., 2018, Journal of Industrial and Engineering Chemistry, 62, pp.26-39.
[4] Khojasteh, D., Kazerooni, M., Salarian, S., Kamali, R., 2016, Journal of Industrial and Engineering Chemistry, 42, pp.1-14.
[5] Khojasteh, D., Bordbar, A., Kamali., Marengo, M., 2017, International Journal of Computational Fluid Dynamics, 31 (6-8), pp.310-323.
[6] Bordbar, A., Taassob, A., Khojasteh, D., Marengo, M., Kamali, R., 2018, Langmuir, 34(17), pp.5149-5158.
[7] Mele, E., Bayer, I.S., Nanni, G., Heredia-Guerrero, J.A., Ruffilli, R., Ayadi, F., Marini, L., Cingolani, R., Athanassiou, A., 2014, Langmuir, 30 (10), pp.2896-2902.
[8] Khojasteh, D., Kazerooni, N.M., Marengo, M., 2018, Journal of Industrial and Engineering Chemistry, 71, pp. 50-64.
[9] Khoufech, A., Benali, M., Saleh, K., 2015, Powder Technology, 270, pp.599-611.

[10] Dehghan Manshadi, M.K., Khojasteh, D., Mohammadi, M., Kamali, R., 2016, International Journal of Numerical Modelling: Electronic Networks, Devices and Fields, 29 (5), pp.845-858.
[11] Khojasteh, D., Dehghan Manshadi, M.K., Mousavi, S.M., and Kamali, R., 2016, Droplet Impact on Superhydrophobic Surface under the Influence of An Electric Field. 3rd Annual International Conference on New Research Achievements in Chemistry & Chemical Engineering, Tehran, Iran.
[12] Wang, Z., Lopez, C., Hirsa, A., Koratkar, N., 2007, Applied physics letters, 91 (2), p.023105.
[13] Kim, H., Lee, C., Kim, M.H., Kim, J., 2012, Langmuir, 28(30), pp.11250-11257.
[14] Moevius, L., Liu, Y., Wang, Z., Yeomans, J.M., 2014, Langmuir, 30 (43), pp.13021-13032.
[15] Akao, F., 1980, Trans. Int. Steel Inst. Japan, 20, pp.737-743.
[16] Scheller, B.L., Bousfield, D.W., 1995, AIChE Journal, 41 (6), pp.1357-1367.
[17] Clanet, C., Béguin, C., Richard, D., Quéré, D., 2004, Journal of Fluid Mechanics, 517, pp.199-208.
[18] Roisman, I.V., 2009, Physics of Fluids, 21 (5), p.052104.